Journal of Mining and Environment (JME), Vol. 14, No. 3, 2023, 731-754

Shahrood University of Technology

Journal of Mining and Environment (JME)

Journal homepage: www.jme.shahroodut.ac.ir

Iranian Society of Mining Engineering (IRSME)

A Study on Seismic Analysis of Underground Tunnels for Delhi Metro

Rahul Shakya* and Manendra Singh

Department of Civil Engineering, National Institute of Technology Hamirpur, Himachal Pradesh, India

Article Info

Received 11 January 2023
Received in Revised form 1 April 2023
Accepted 4 June 2023
Published online 4 June 2023

DOI:10.22044/jme.2023.12598.2289

Keywords

Seismic analysis
Numerical model
Finite element method
Uttarkashi Earthquake

Abstract

Due to fast urbanization, there is a shortage of above-ground surfaces. Thus to reduce this shortage of above-ground surface, underground tunnels are constructed beneath the structure for transportation purposes. As a result, it is critical to understand how earthquakes affect underground tunnels, so that people's lives can be saved and service levels can be maintained. Underground constructions cannot be considered entirely immune to the impacts of ground shaking, as evidenced by the Kobe earthquake (1995), the Chi-Chi earthquake (1999), and the Niigata earthquake (2004), when some underground structures were severely damaged. A typical section at Chandani Chowk of DMRC (Delhi Metro Rail Corporation) tunnels, New Delhi, India, has been analyzed by using the finite element method. Response of the soil tunnel system for the Uttarkashi earthquake (1991) has been found out in the form of maximum forces induced in the RC liner of the tunnel, displacement, induced acceleration and stresses. The results have been compared with the available closed-form solutions. Parametric studies by considering different parameters such as effect of contraction (volume loss), influence of boundary conditions and damping, effect of interface condition between soil and tunnel, effect of displacement time history and effect of a nearby building have also been conducted. Forces in RC liners and stress concentration obtained in the present study are well-matched to those obtained by available closed formed solutions. The vertical stress concentration and volume loss depend upon the soil medium's constitutive behavior. The section under consideration was safe against the 1991 Uttarkashi earthquake. It can also be observed that, due to the presence of the building, the axial force and bending moment increased in tunnel's liner, and the value of all three forces reduced as the position of the building was away from the tunnel. Shear force and bending moment were maximum for full slip condition between soil and tunnel lining however the effect of the interface condition on the displacement was negligible after a certain value of the interface condition.

1. Introduction

Fast population growth in urban areas has resulted in a significant need for ground space. As above-ground surface in urban areas is limited, sub-surface structures such as tunnels are becoming more efficient for fulfilling these requirements. Large underground gas and petroleum storage facilities near major geological discontinuities, the water conductor systems of hydropower projects, roadways and railroad tunnels in hilly terrain, and other underground structures are common in transportation and utility networks. In 1863, the first underground railway system was established in London, and more than 30,0000 people decided to travel on its first day of operation, which was termed "the great engineering triumph of the day." As of January 2021, approximately 204 metro systems serve about 205 cities in 61 countries. The development and operation of these systems may restrict services and cause surface and subsurface damage. Historically, underground constructions subjected to seismic loads suffered a lower rate of damage than above-ground ones [1]. As a result, it was anticipated that underground structures such as tunnels would be immune to seismic activity. Nonetheless, if a tunnel near an earthquake fault

* *Corresponding author: rahulshakya4050@gmail.com (R. Shakya)*

encounters a significant tremor, there is a considerable likelihood that the tunnel will be damaged. Table 1 displays the tunnel's performance over the previous few years due to the earthquake.

Table 1. Damages to tunnels by earthquakes over the past years [2].

Year	Location	Magnitude	Tunnel's performance
1906	San Francisco	8.3	Two tunnels that cross the San Andreas fault have suffered severe and extensive damage
1923	Kanto (Japan)	7.9	More than 100 tunnels were affected
1927	Kita-Tango	7.3	Very slight damage occurs
1930	Kita-Izu	7.3	Severe damage shown by tunnels
1948	Fukui (Japan)	7.1	Severe damage within 8 km of the earthquake
1952	Tokachi-Oki	8.2	Slight damage to 10 railway tunnels
1952	Kern (USA)	7.7	Severe damage to 4 railway tunnels
1961	Kita-Mino	7	Cracking occurs in tunnels
1964	Niigata	7.5	20 railway tunnels affected
1970	Tonghai	7.7	Severe damage to road tunnels
1971	Los Angeles	6.6	Several damages to mountain tunnels
1978	Miyagiken	7.4	Slight damage to 6 railway tunnels
1982	Urakawa-Oki	7.1	Slight damage to 6 railway tunnels
1984	Naganoke	6.8	Cracking damage to one hydraulic power
1987	Chibaken	6.7	Damage to the wall of one railway tunnel
1995	Hyogoken	7.2	Damage to over 20 tunnels
1999	ChieChi (Taiwan)	7.6	14 were severely damaged, 11 were moderately damaged, and 23 were slight damage
2004	Niigataken	6.8	About 50 tunnels were damaged
2007	Niigataken Chuetu-Oki	6.8	Damage to about 21 tunnels
2008	Wenchuan	8.0	Underground transportation and other infrastructures were severely damaged
2015	Gorkha, Nepal	7.8	More than 150 damages were found along the melamchi tunnel
2016	Kumamoto	7.3	Severe damage to mountain tunnel

2. Literature Review

In comparison to structures built on the ground's surface, those constructed underground are assumed to be less vulnerable to the influence of earthquakes. However, earthquakes can cause severe damage to some subsurface structures. Hence, underground constructions cannot be regarded as fully safe. The Daikai subway station was the first underground structure to collapse directly from earthquake forces instead of ground instability. Earthquake effects on underground structures can be grouped into two categories: (1) ground shaking and (2) ground failures such as liquefaction, fault displacement, and slope instability. Liquefaction, slope instability, and fault displacement are all examples of ground failure caused by seismic shaking. Ground failure is especially common in shallow tunnels and near tunnel portals. When ground failure is present, special design considerations are required. Because of the interaction of seismic waves with surficial soft deposits and the generation of surface waves, deformation can be quite complex. Underground structures can therefore be assumed to deform in three ways during seismic shaking: (1) axial, (2) curvature, and (3) ovaling (for circular tunnels) or racking (for rectangular tunnels) when seismic waves propagate parallel or obliquely to a horizontal or nearly horizontal linear tunnel, axial and curvature deformations predominate [1]. For these deformations, tunnel lining design considerations are primarily in the longitudinal direction along the tunnel axis. Figure 1 depicts idealized representations of axial and curvature deformations.

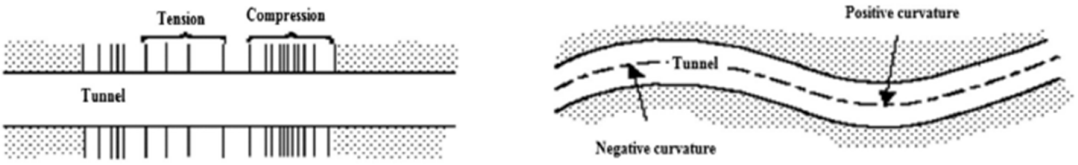

a) Axial deformation **b) Curvature deformation**

Figure 1. Axial and curvature deformation [3].

When waves propagate in a direction perpendicular or nearly perpendicular to the tunnel axis, the cross-sectional shape of the tunnel lining is distorted, resulting in ovaling or racking deformations. Transverse design considerations must be considered when dealing with this type of deformation. Figures 2 and 3 show the ovaling and racking distortions in circular and rectangular tunnels, respectively.

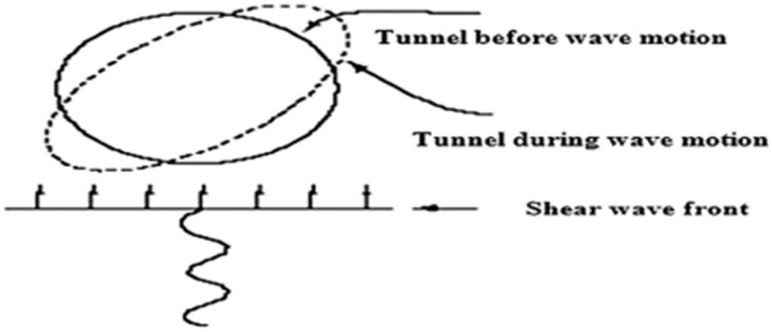

Figure 2. Ovaling deformation [3].

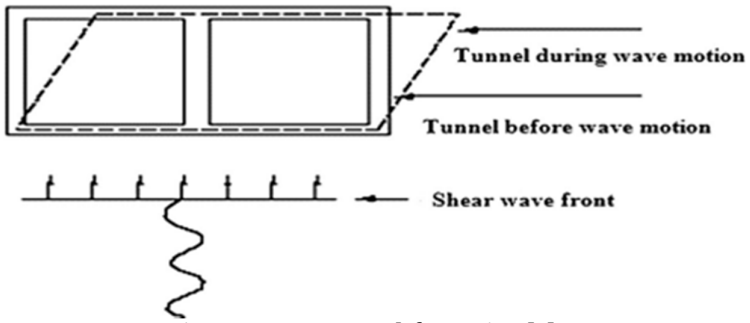

Figure 3. Curvature deformation [3].

Several methods for evaluating the seismic response of underground structures and tunnels are available in the literature [4-8]. Several experimental research studies have been recently carried out to understand better these structures' seismic behaviour [9-11]. Xu *et al*. [12] have performed an experimental study (shaking table test) for the dynamic response of tunnels under seismic vibrations. In the experimental research, some researchers modelled the tunnel using an either slurry of gypsum and water [12], reinforced concrete [13, 14] micro-concrete, reinforced with steel mesh or polypropylene fibres [15] or organic glass [16]. From the technical perspective of civil engineering, Chen *et al*. [17] studied the based-on failure mode, damage mechanism, seismic design method, prevention measures and post-earthquake repair of tunnels. Tsinidis *et al*. [18] discuss the seismic response of circular tunnels in dry sand and investigates the efficiency of current seismic analysis methods at extreme lining flexibilities. Initially, a dynamic centrifuge test on a flexible circular model tunnel embedded in dry sand is analyzed by means of rigorous, complete dynamic analysis of the coupled soil–tunnel system, applying various nonlinear soil and soil–tunnel interface models.

Currently available methods of shaking design typically assume free field conditions, excluding above-ground structures in the tunnel's adjacent area. On the other hand, tunnels in urban areas are frequently built beneath or very near tall buildings. During an earthquake, the vibration of these above-ground structures might cause complicated interaction phenomena with the tunnel, which often passes just a few meters below their foundation. The seismic wave propagation field is expected to be affected by these interactions. These changes allow them to influence the dynamic reaction of the tunnel, as well as alter the structure's dynamic response due to its proximity to the surface and foundations. Both factors may modify the dynamic response. When it comes to the dynamic interaction phenomena between above-ground and embedded structures, most researchers focus on the effect that an underground structure, typically a circular tunnel or a cavity, has on the response of the above-ground structures. Sharma *et al*. [19] expanded on the earlier authors' collection, reaching 192 cases involving 85 earthquakes. To link the seismic susceptibility of a tunnel to some significant elements, 6 criteria were looked at: the tunnel cover, the subsoil type [20], the peak ground acceleration [21-24], the size of the earthquake [2], the distance from the epicentre, and the type of support system. The reported damage decreases as the depth of the overburden increases. The magnitude and epicentral distance of the affecting earthquake may influence damage. Rowe [25] investigated the effects of earthquake waves, hard rock, faults, and liquefaction on tunnels. When a tunnel crosses an active fault, it may sustain serious damage due to differential displacements incompatible with the structure's strength. The level of damage was discovered to be a function of fault displacement, lining, and rock condition; tunnels in soft soil or soft rock layers were more vulnerable to damage. Experimental results from sand tunnel centrifuge models subjected to seismic loading were examined by Lanzono *et al*. [26], who then compared their findings to predictions from finite element dynamic analysis and other simplified approaches. When cyclic shear strains are properly evaluated, analytical formulations provide a good estimate of the bending moment in the lining and a reasonable lower bound for transient changes in hoop forces. The two-dimensional seismic behaviour of a circular tunnel was studied by Pakbaza *et al*. [27] using the finite difference method, and they found that the impact of an earthquake on tunnel-ground interaction is dependent on several parameters such as the peak acceleration, the intensity, and duration of the earthquake. Rapid response and repair of underground tunnels after earthquake disasters are essential requirements for urban infrastructures to achieve resilience. Hence, research on the seismic resilience of underground tunnels is very important topic for research [28-33].

There are also closed-formed solutions for seismic analysis in the literature, as presented by Wang [8], Penzien and Wu [34], Penzien [5], and Hashash *et al*. [1, 35]. Due to racking deformation, Penzien and Wu [34] found analytical solutions for thrust (axial Force), shear Force, and bending moment in the tunnel lining. Penzien [5] later included a supplemental analytical approach for evaluating racking deformation in rectangular and circular tunnels. Hashash *et al*. [1,35] observed that the computed forces and displacements are equal for the full-slip assumption. However, Penzien's approach resulted in a substantially lower calculation of maximum thrusts than Wang's solution for the no-slip assumption. Under seismic loading, Wang [8] is credited with being the first to present a closed-form solution for internal forces in the tunnel lining structure in the no-slip and full-slip states. Wang, on the other hand, did not propose a solution for calculating bending moments under no-slip conditions, instead recommending that no-slip situations be solved using full-slip condition solutions.

3. Problem Definition

As part of India's massive infrastructure expansion, metro underground construction as a mass rapid transport system has begun in numerous metropolitan areas. According to a 2021 report, a total of 2.63 billion people travel annually in metro systems across India's 13 major cities, making India one of the busiest urban rapid transit hubs in the world regarding ridership. India has the fifth-longest operating metro system in the world, with a total length of 751.50 kilometers [36].

The capital of India was relocated from Kolkata to Delhi in 1911. This resulted in massive urban sprawl, increasing the city's population by magnitude. When a traffic and travel characteristics study was conducted in 1969, the first concept of an urban rapid transit system was developed [37]. The bus systems that provided public transportation in the city exacerbated traffic congestion, quickly becoming a growing concern. So, after planning, a proposal was made in 1984 that revealed plans for three underground corridors and the expansion of the existing suburban rail

system. The first line was operational on December 24, 2002, after construction began on October 1, 1998. With 348.12 kilometers of track, the Delhi Metro became India's longest and busiest metro system.

Most underground metro tunnels in Delhi's capital city are shallowly buried. Since shallow tunnels are more prone to damage during an earthquake, it is necessary to ascertain their seismic response to earthquake loading. Figure 4 shows the typical portion of DMRC (Delhi Metro Rail Corporation) tunnels constructed at Chandani Chowk that has been taken for analysis in this study. It serves the very busy commercial area of Chandni Chowk in Old Delhi, India. The entire problem was simulated in PLAXIS 2D, and a dynamic analysis utilizing finite element modelling was undertaken to comprehend the seismic behavior of the underground tunnel by considering the Uttarkashi earthquake in 1991.

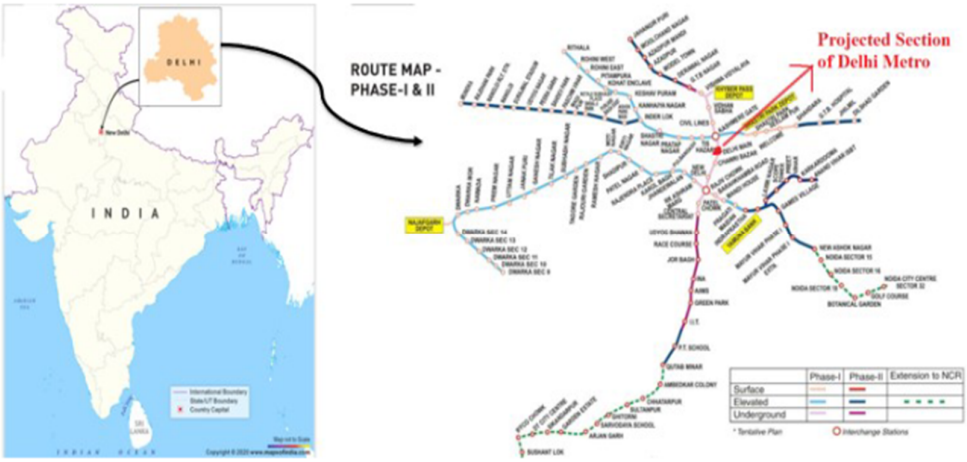

Figure 4. Studied area and alignment plan for phase-I and phase II of the Delhi Metro project [38].

4. Numerical Model Development

A two-dimensional plane strain dynamic finite element analysis with a rectangular domain (128 x 78 m) was used to evaluate the forces in tunnel lining. Plaxis 2D software was used for analyzing the problem. 15-noded triangular elements were used for discretizing the soil mass. The constitutive behaviors of the subsoil are assumed to be linear elastic. The RC liners were modeled using 32 plate bending elements and assumed to be elastic and impervious. All geometric properties have been adopted from [38, 39] for the present study. Figure 5 shows the geometry of the physical model of the site.

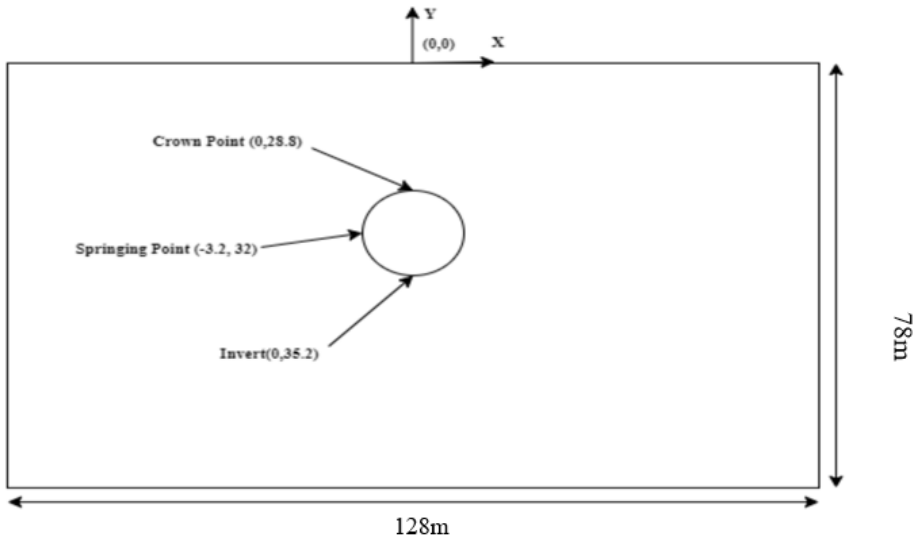

Figure 5. Geometry of physical model (Chandani Chowk).

The DMRC tunnel in Chandani Chowk has a diameter of 6.4 m and an overburden depth of 28.8 m. Reinforced Concrete (RC) liners with a thickness of 0.28 m have been used as a permanent support system. Modulus of Elasticity (E_c) and Poisson's were 3.16 x 10^7 kPa and 0.15 for RC liners, respectively. Alluvium deposits, also called "Delhi silt," were found digging tunnels for the DMRC. The value of Delhi Silt's elastic modulus changes with depth, as shown in Equation (1).

$$E = 1.22 + 0.83(z) \quad (1)$$

where z is the depth of the soil layer.

Delhi silt's in-situ unit weight and saturated unit weight were 18.33 kN/m^3 and 21.35 kN/m^3, respectively. During the digging of the tunnel, no water table was found. Cohesion, c, of Delhi silt has been taken as 0. The friction angle was 35°, and the dilatational angle was found to be 5°. No slip has been assumed between the soil around the tunnel and the RC liners that hold it up. The value of damping in the soil and RC liners was taken as 5% and 2%, respectively. Plaxis makes use of Rayleigh damping in the seismic analysis. Rayleigh damping has been calculated by using Equation 2.

$$C = \alpha M + \beta K \quad (2)$$

where,

M = Mass matrix

K = Stiffness matrix

α and β = Rayleigh damping coefficients

α and β are determined by using Equation 3.

$$\begin{Bmatrix} \alpha \\ \beta \end{Bmatrix} = \frac{2\xi}{\omega_m + \omega_n} \begin{Bmatrix} \omega_m \omega_n \\ 1 \end{Bmatrix} \quad (3)$$

where ξ is the damping ratio, and ω_m, ω_n are natural frequencies of soil mass in rad/sec corresponding to mode shapes, m and n, respectively.

4.1. Seismic loading

Delhi and its surroundings have experienced earthquakes since ancient times. Mahabharata's great epic mentions earthquakes (Circa 3000 BC) during the war at Kurukshetra [40]. There have been seismic events in Delhi in the past; Table 2 shows the list of some recent earthquakes in Delhi.

Table 2. Recent Earthquakes in Delhi [41].

Date	Magnitude
06/06/1992	2.8
16/02//1993	2.6
27/03/ 1993	3.6
06/08/1993	2.5
3/12/1993	3.5
28/07/1994	2.8
15/10/1994	2.8
16/11/1994	2.9
18/03/2004	2.7
05/04/2004	1.9
21/04/2004	1.5
06/06/2004	2.0
25/11/2007	4.1
07/09/2011	4.2
05/03/2012	4.9
24/04/2018	3.5
20/12/2019	6.3
13/04/2020	2.7

Since no significant earthquake occurred in Delhi, this study will focus on the lower Himalayan earthquake of 1991 in Uttarkashi. On the Richter scale, the earthquake had a magnitude of 6.8. The horizontal component's time history of this earthquake was used in this study and is shown in Figure 6 after applying the baseline correction factor. This earthquake's peak ground acceleration (PGA) was 3.04 m/sec^2 (0.309 g). The model's base was subjected to an earthquake. Newmark's (1986) time integration method was employed in this investigation.

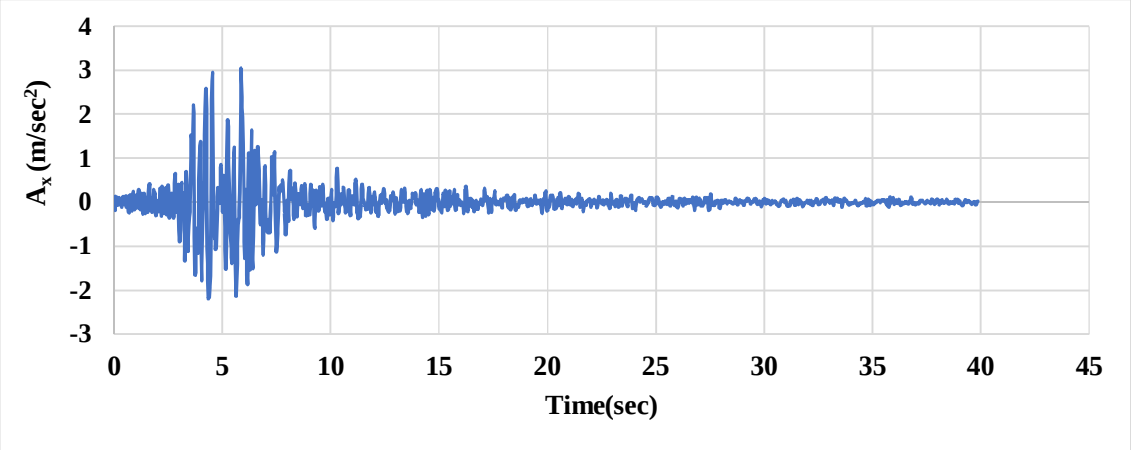

Figure 6. Horizontal acceleration (A_x) – time history of Uttarkashi (1991) earthquake.

4.2. Boundary conditions

It is necessary to pick suitable dynamic boundary conditions to replicate real conditions and generate meaningful findings accurately. Nodes on the finite element mesh's vertical boundaries were restricted in the X direction but free to move in the Y direction for static conditions. Nodes on the mesh's bottom boundary were restricted in both X and Y directions. In the dynamic condition, non-reflecting (absorbing) boundaries were used along the vertical boundaries.

Non-reflecting (absorbent) boundaries, also called viscous boundaries, were utilized to represent displacement along both vertical boundaries to prevent seismic waves from being reflected into the model after reception at these boundaries, as recommended by Lysmer and Kuhlmeyer [42].

Every node along the viscous boundary has a dashpot for each degree of freedom. Equations (4) and (5) describe the normal and shear forces absorbed by a damper in the X-direction.

$$F_n = a.A.\rho V_p \dot{u_x} \quad (4)$$

$$F_t = b.A.\rho V_s \dot{u_y} \quad (5)$$

where ρ is the density of the material, and the compressional and shear wave velocities are V_p and V_s, respectively, and $\dot{u_x}$ and $\dot{u_y}$ represent the particle velocities normal and tangential to the boundary. '*A*' stands for the node's associated area, and a and b are taken as unity for full absorption. Experimental and numerical research has shown that the boundary does not completely absorb shear waves. Hence the parameter b should be set at 0.25 based on previous experience. In this investigation, 'a' and 'b' were taken to be 1 and .25, respectively.

5. Results and Discussion

The tunnel's response to the 1991 Uttarkashi earthquake in the lower Himalayas has been studied by conducting a seismic analysis. Figure 5 depicts the geometry of the physical model that incorporates the soil layers and the tunnel that has been treated as already built. It displays the X–Y coordinate system used as a reference and various monitoring points, such as the crown, invert, and springs.

5.1. Soil-tunnel's response to seismic load

The Delhi Metro tunnel was analyzed using 5% soil mass damping and 2% RC liners damping for the horizontal component of the Uttarkashi earthquake. For discussion, here are the findings of the linear elastic analysis.

Ovaling deformation of circular tunnels

When waves travel perpendicular to the tunnel axis, ovaling deformation occurs. For the vast majority, previous studies have found this deformation caused by vertically propagating shear waves however in present study acceleration *vs.* time histories was used for determining stresses, displacement and forces. Figures 7 and 8 show the deformed mesh of the model before the earthquake and after the earthquake, respectively. It also shows the maximum displacement before the earthquake (0.02660m) and after the earthquake (0.1260 m). Therefore, maximum displacement has increased significantly due to earthquake.

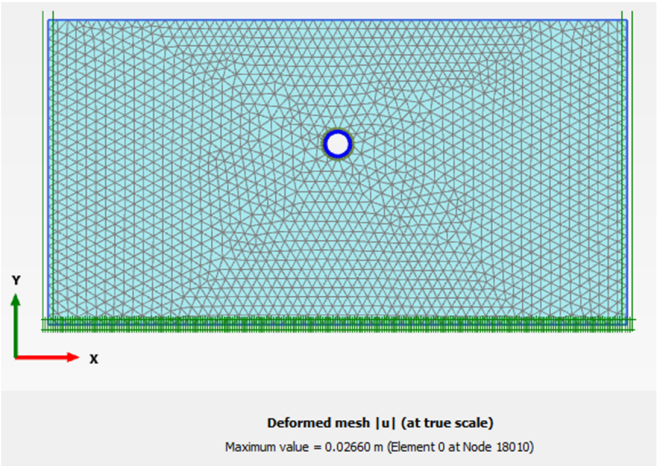

Figure 7. Deformed mesh before the earthquake (extreme total displacement = 0.02660 m).

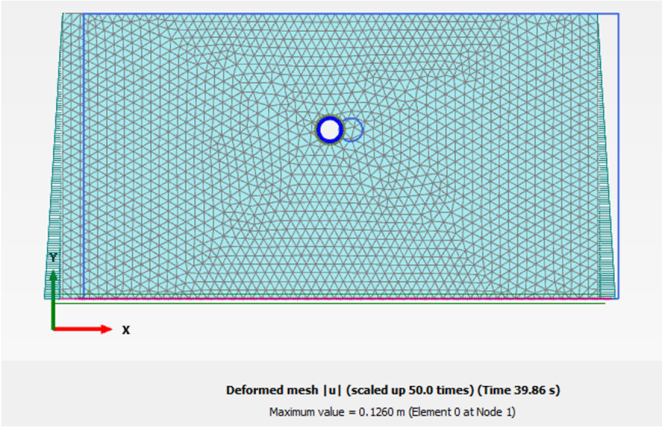

Figure 8. Deformed mesh at the end of 1991 Uttarkashi earthquake.

Dynamic forces in RC liners of tunnels

The induced axial Force, shear Force, and bending moment in RC liners are tabulated in Table 3. During shaking, the axial Force is virtually constant along the periphery of the tunnel as shown in Figure 9-a, with a maximum value of 2136 kN/m, and the residual axial force is determined to be 2071 kN/m at the end of shaking, as shown in Figure 9-b. Shear Force ranges considerably along the periphery of RC liners, with the maximum shear Force occurring halfway between the crown and the springing point and having a magnitude of 181.9 kN/m during shaking, as shown in Figure 9-c. The residual shear Force was determined to be 128.8 kN/m at the end of shaking, as shown in figure 9-d. When it comes to the bending moment, it has been discovered that it changes significantly along the liner's periphery. During an earthquake, the maximum bending moment in liners occurs at the tunnel's spring point, with a value of 290.4 kN-m/m length of the liner, as shown in Figure 9-e, whereas the residual value of the bending moment is 200.6 kN-m/m, as shown in Figure 9-f.

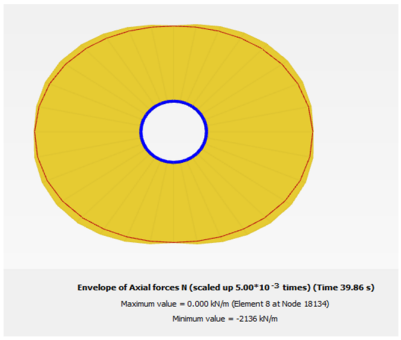

a). Maximum axial force during EQ.

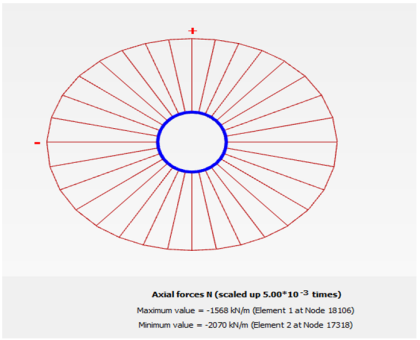

b. Residual Axial Force. during EQ.

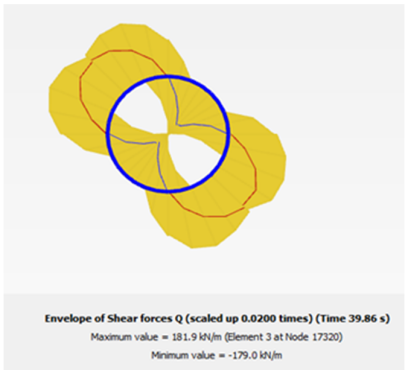

c. Maximum Shear Force during EQ.

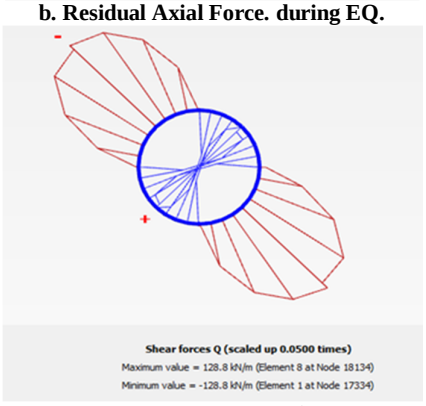

d. Residual Shear Force after EQ.

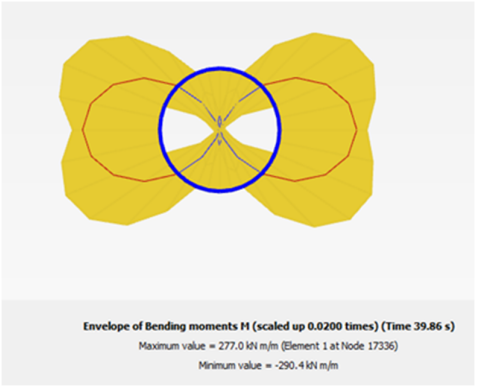

e. Maximum Bending Moment during EQ.

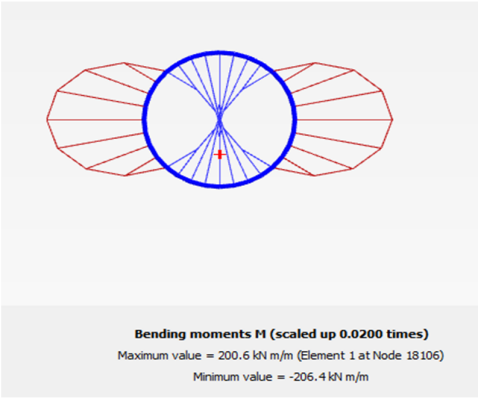

f. Residual Bending Moment after EQ.

Figure 9. Axial force, shear force, and bending moment in RC lining.

Table 3. Extreme forces in RC liner due to the horizontal component of the Uttarkashi earthquake.

Dynamic forces in RC liner	Static	During shaking	After shaking
T(kN/m)	2070	2136	2071
M(kN-m/m)	206.4	290.4	206.5
V(kN/m)	128.8	181.9	128.9

It can be seen in Table 3 that the axial force varies just slightly throughout the earthquake compared to the static situation but shear Force and bending moment, on the other hand, have increased by around 1.4 times their static value during the earthquake and subsequently decrease to the same level (approximately) as the static state at the end of the earthquake. The combined axial Force and bending moment stress in RC liners are 21.54 MPa, lower than the permissible stress in M40 concrete (23 MPa as per [43]). Forces in RC liners increase dramatically during the earthquake, yet stresses in RC liners do not exceed their acceptable range, according to the analysis. Even though this conclusion cannot be applied to all earthquakes, these tunnels may react very differently to a stronger earthquake in the Delhi area with a different peak ground acceleration or frequency content. Depending on how the earthquake moves, these tunnels could be damaged. Also, keep in

mind that this is only a linear study. If the soil mass's non-linearity was considered, the actual stresses and deformations might differ. The analysis has also been done by changing the input wave into the FEM model for 5%, 10%, and 15% damping ratios. Figure 10 shows the combined stresses in the liner of the tunnel at 0.3g (a_{max} during the Uttarkashi earthquake), 0.36 g (1.2*a_{max}), 0.39 g (1.3*a_{max}), 0.45 g (1.5* a_{max}), and 0.51 g (1.7*a_{max}). The result shows that the combined stresses in the RC liner (M40 concrete) of the tunnel cross the permissible limit at .36 g (5% damping), 0.45 g (10% damping), and 0.51 g (15% damping). It can also be concluded from Figure 10 that for the damping ratio of soil 5 %, 10%, and 15%, this section of tunnel was found to be safe against the earthquake having acceleration up to 0.3 g, 0.39 g, and 0.45 g, respectively. Therefore, this tunnel section can resist the earthquake of acceleration 0.5 g if soil damping is 15%.

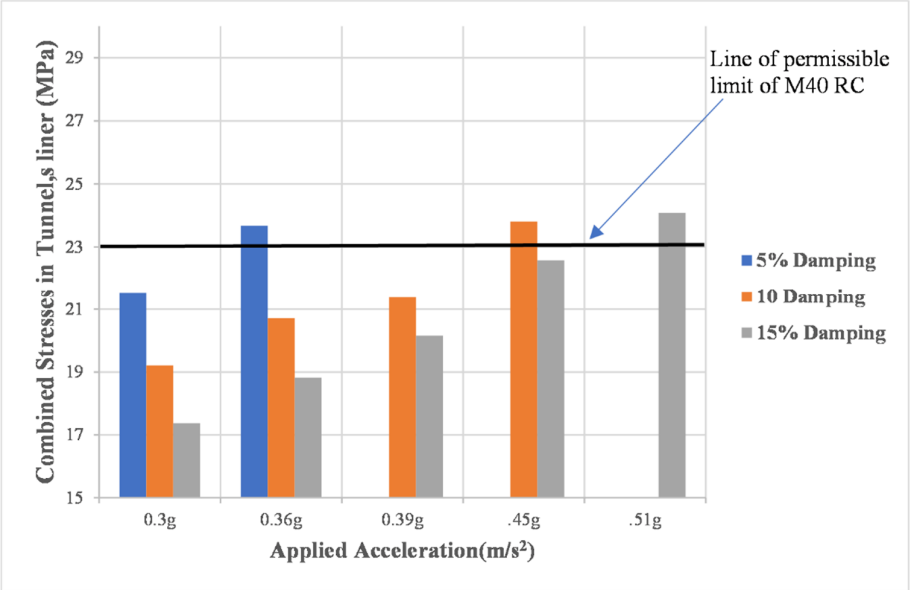

Figure 10. Combined stresses in RC liner at different damping ratios.

5.2. Comparison of numerical solution to analytical solution

The seismic response of the Delhi metro underground tunnel due to seismic loading (Uttarkashi Earthquake,1999) has been calculated using the closed-form solutions in this study. For full slip condition between soil and tunnel, Wang [8] has published explicit equations for diametric strain, axial Force, and bending moment in RC liners of the tunnel. In contrast, Penzien and Wu [34] and Penzien [5] have presented equivalent solutions for both full and no-slip conditions (Appendix B).

Table 4 shows the value of the maximum Force induced in the RC liner during the seismic loading (Uttarkashi earthquake, 1991). The comparison of these values has been made with the available closed-form solution. From Table 4, it can be seen that forces in RC liners obtained in the present study are well-matched to those obtained by Penzien and Wu (1998) and Penzien (2000). There are no significant differences between the results obtained by Wang [8], Penzien and Wu [34], and Penzien [5] in terms of axial thrust or bending moment for full slip; Wang's approach overestimates the axial thrust for no-slip condition and PLAXIS yields nearly identical results for the bending moment and shear Force developed in RC liners.

Table 4. Maximum dynamic forces in RC liners.

Dynamics forces in RC liner	Wang		Penzein and Wu Penzien		Present study using PLAXIS, no slip
	Full Slip	No-Slip	Full Slip	No Slip	
T(kN/m)	28.81	89.07	28.81	54.08	66
M(kN-m/m)	92.19	-	92.20	86.53	84
V(kN/m)	-	-	57.62	54.08	53.1

5.3. Parametric study

At this point, an attempt has been made to carry out some parametric analysis, mainly focusing on the influence of damping of soil mass, the influence of volume contraction, and the effect of a nearby building on the forces mobilized in RC liner of the tunnel and the kind of boundary simulation that was employed.

5.3.1. Effect of contraction (volume loss)

The ratio of final vertical stress (stress after the tunnel's construction) to the initial stress (stress before the tunnel's construction) at any point surrounding the tunnel is known as vertical stress concentration. Figure 11 shows the vertical stress concentration along the horizontal axis of the tunnel. It can be observed that the vertical stress concentration has the maximum value at r/a = 1, then it starts to decrease up to r/a = 4, and after that, it becomes constant. From Figure 8, it can be concluded that vertical stress concentration increases with an increase in volume loss, especially near the periphery of the tunnel. The results have been compared with Terzaghi and Richart's [44] (Appendix-A) solutions, as shown in Figure 11. It can also be concluded from Figure 11 that the PLAXIS model has the same value of vertical stress concentration as Terzaghi and Richart [44] for volume contraction of 2%. Therefore, a volume loss of 2% for this site should be taken for the elastic analysis.

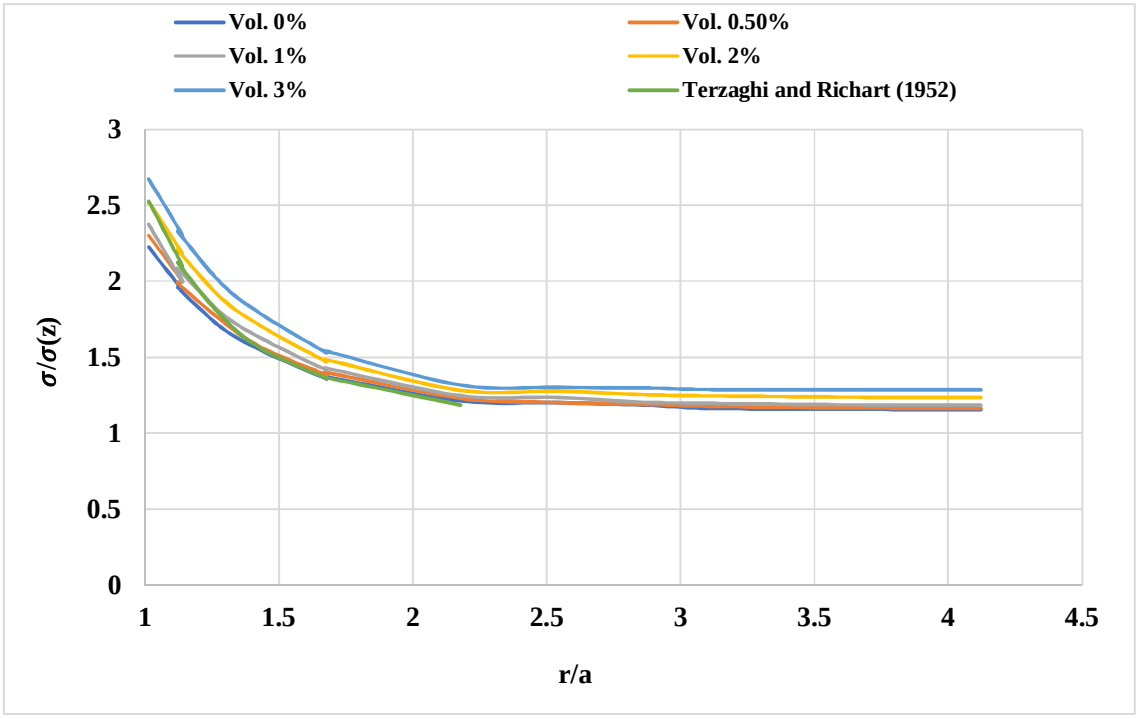

Figure 11. Vertical stress concentration along the horizontal axis of the tunnel. (where 'a' and 'r' are the radius of the tunnel and radial distance along the tunnel's axis, respectively).

Table 5 represents the maximum horizontal displacement (U_X) and vertical displacement (U_Y) in the soil and the tunnel for different values of volume contraction. Table 5 shows that the maximum displacement in soil remains constant, whereas settlements in the tunnel increase slightly with an increase in the value of volume contraction.

Figure 12 shows the variation of vertical stress concentration along the tunnel's horizontal axis for the soil elastoplastic behavior. From Figure 12, it can be concluded that the soil nearby the surrounding tunnel entered the plastic zone, and the value of the vertical stress concentration ratio dropped down less than unity. The value of this factor ratio has increased to the maximum value up to a certain distance from the tunnel, and this distance is known as elastoplastic radius. Beyond the elastoplastic radius, the stress concentration value decreased up to a certain distance and became constant at a distance far away from the tunnel. It can also be observed from Figure 12 that for the volume contraction of 3%, the stress concentration factor ratio follows the trend with Bray's closed-form solutions [45]. Therefore, for this site, a volume loss of 3% should be taken for the elastoplastic analysis.

Table 5. Maximum displacement in soil-tunnel system elastic behavior of soil.

V_L (%)	Soil		Tunnel	
	U_X (mm)	U_Y (mm)	U_X (mm)	U_Y (mm)
0	19.31	66.39	18.99	67.59
0.5	19.31	66.39	19.37	67.95
1.0	19.31	66.39	19.75	68.32
2.0	19.31	66.39	20.5	69.04
3.0	19.31	66.39	21.34	69.77

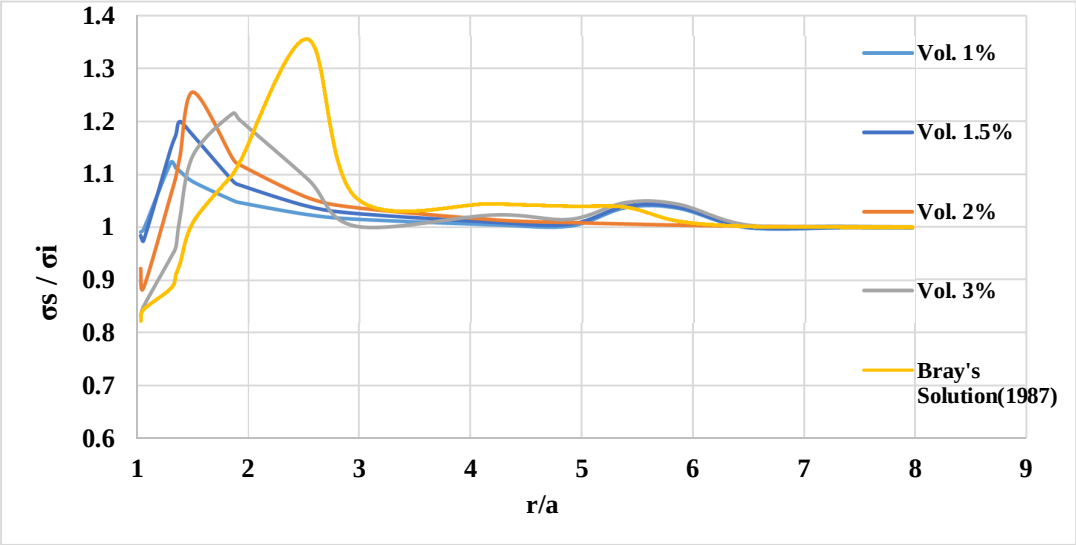

Figure 12. Vertical stress concentration along the horizontal axis for the elastoplastic behavior of the soil.

The values of maximum displacements in the soil and the tunnel for different values of volume contraction have been tabulated in Table 6. Table 6 shows that the maximum displacements in soil and tunnel have increased significantly with an increase in volume loss.

Table 6. Maximum displacement in the soil-tunnel system for elastoplastic behavior of soil.

V_L (%)	Soil		Tunnel	
	U_X (mm)	U_Y (mm)	U_X (mm)	U_Y (mm)
1.0	8.6	56.97	17.21	56.06
1.5	13.11	60.46	20.16	60.27
2.0	21.66	63.67	25.01	64.43
3.0	38.53	70.79	38.52	72.08

Table 7 represents the value of the RC liner's force with and without applying the contraction to the tunnel's face. There is a sudden increment in the value of axial Force by applying the contraction, but in the shear force and bending moment, a slight change occurs. It can be concluded that the maximum effect of using contraction is more on axial force compared to the other RC liner's forces.

Table 7. Maximum dynamic forces in RC liner due to contraction

Dynamic forces in RC liner	Present study using PLAXIS, no slip	
	without contraction	With contraction
T(kN/m)	66	640
M(kN-m/m)	84	81.6
V(kN/m)	53.1	52.1

5.3.2. Influence of boundary conditions and damping

Changes in the soil's damping value and using elementary boundaries with 0% damping were also used to analyze the soil tunnel system. In this study, three different values of the damping ratio were used for the parametric study: 0%, 5%, and 10%. Table 8 shows that the value of axial Force, shear Force, and bending moment decreases as the value of the soil's damping decreases. Still, the change in axial Force was marginally affected by the damping compared to the shear Force and bending moment, as the previous researcher also found. The maximum influence of damping on the axial Force was recorded during the 0%-5% damping range.

The soil-tunnel system without absorbent boundaries with 0% damping was also analyzed to determine the influence of boundaries on the value of the RC liner's forces. From Table 8, there is an increment in the value of the RC liner's forces by using the system without absorbent boundaries. It occurs due to the reflection of waves from the boundaries of the model and again hitting on the RC liner but with a very low velocity. It can also be concluded that when any FEM model was analyzed without boundaries, then the domain of the model should be large so that the reflection of the wave cannot occur.

Table 8. Maximum dynamic forces in RC liner due to type of boundaries with different values of damping ratio.

Maximum forces in RC liner	Static	During an earthquake with absorbent boundaries			During the earthquake, without absorbing boundaries
		0% damping	5% damping	10% damping	0% damping
T(kN/m)	2070	2136	2085	2080	2158
M(kN-m/m)	206.4	290.4	221.6	213.3	314.7
V(kN/m)	128.8	181.9	139.8	133.9	190.2

5.3.3. Effect of interface condition between soil and tunnel

Finite element modelling of soil and structure interactions encounters the problem of displacement discontinuity across the boundaries of two different materials, which could be solved by placing interface elements along the boundaries [46]. To model soil-structure interactions and capture the transfer of normal and shear stresses through these discontinuities, interface elements between dissimilar component materials are typically used in numerical study of soil-structure interaction. Without an interface the structure and the soil are tied together: no relative displacement (slipping/gapping) is possible between structure and soil. Numerical software programs (Plaxis-2D) have interface models to simulate soil-structure interactions [47, 48] using zero-thickness interface elements [49, 50]. These programs give similar numerical outcomes of normal and shear stresses at the interfaces between the soil and structures [51]. Using "zero-thickness" interface elements between soil and structural components, finite element method software tools (Plaxis-2D) can model soil–structure interactions. These components apply a strength/rigidity reduction factor to the soil close to the interface. These interfaces have properties of friction angle (Φ_i), cohesion (C_i), dilatancy angle (Ψ_i) and shear modulus (G_i). The values of interface properties in PLAXIS can be set directly by using a strength/stiffness reduction factor ($0<R_i \leq 1.0$), where 0 represents smooth interface (i.e. no shear strength is developed), and 1 represents rigid interface (i.e., no relative displacement between the dissimilar layers. This factor is applied to the properties of the adjacent soil as follows:

$$C_i = R_i * C_{soil} \quad (6)$$

$$\emptyset_i = tan^{-1}(R_i tan\emptyset_{soil}) \quad (7)$$

$$\psi_i = \begin{cases} 0 & R_i < 1 \\ \Psi_{soil} & R_i = 1 \end{cases} \quad (8)$$

$$G_i = R_i^2 * G_{soil} \quad (9)$$

where,

C_{soil} = Soil cohesion
$\emptyset_{soil}$ = Soil friction angle
G_{soil} = Soil shear modulus
Ψ_{soil} = Soil dilatancy

Displacement in soil medium and tunnel liner

Figure 13 shows the horizontal and vertical displacement in soil medium and in the tunnel liner due to the seismic loading. It can be concluded that the displacement was maximum when the interface condition value was near to 0 (Full-slip condition) and it decreases as the value of R_i increases up to

the value of R_i was 0.4. After that the displacement was found almost constant it means the effect of interface condition after 0.4 was negligible.

Effect of interface on the structural forces in tunnel liner

Figure 14 shows the structural force (axial force, shear force and bending moment) in tunnel liner during the seismic loading. From Figure 14, It can be stated that on increasing the value of interface factor R_i, the axial force induced in the tunnel liner increases slightly, while shear force and bending moment were found to decrease on increasing the value of R_i.

5.3.4. Effect of displacement time history

In this section, displacement time history was applied at the base of model in place of acceleration time history then the comparison of response of soil-tunnel system subjected to displacement time history and acceleration time history has been done. Figures 5 and 6 show the induced acceleration at the ground surface for both time histories with building and without building, respectively, where $(A_x)_a$ and $(A_y)_a$ are induced acceleration at the ground surface in horizontal and vertical direction, respectively, for acceleration time history, and $(Ax)_d$ and $(Ay)_d$ are induced acceleration at the ground surface in horizontal and vertical direction respectively for the displacement time history.

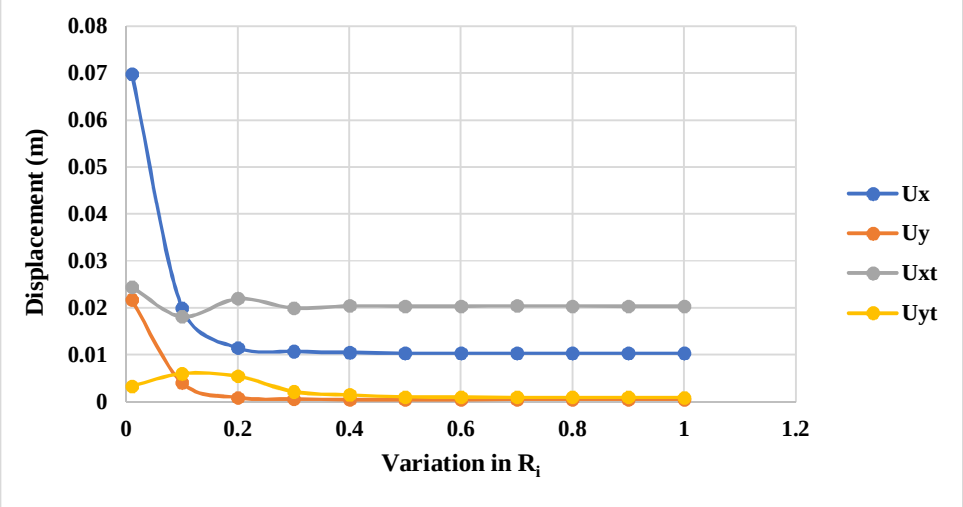

Figure 13. Displacement in soil medium and tunnel liner with different interface condition (where U_x and U_y are the displacement in soil medium in horizontal and vertical direction, respectively; U_{xt} and U_{yt} are displacement in tunnel lining in horizontal and vertical direction, respectively).

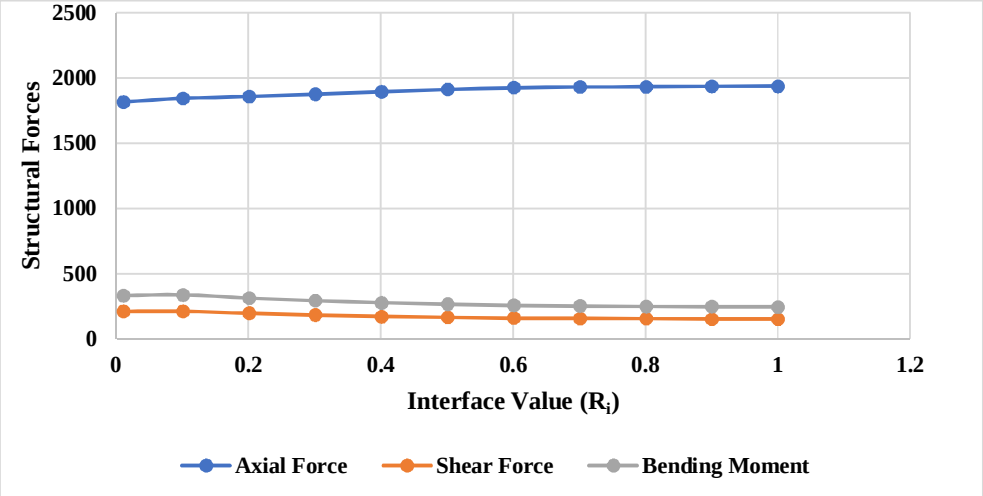

Figure 14. Maximum Structural Force induced in tunnel liner.

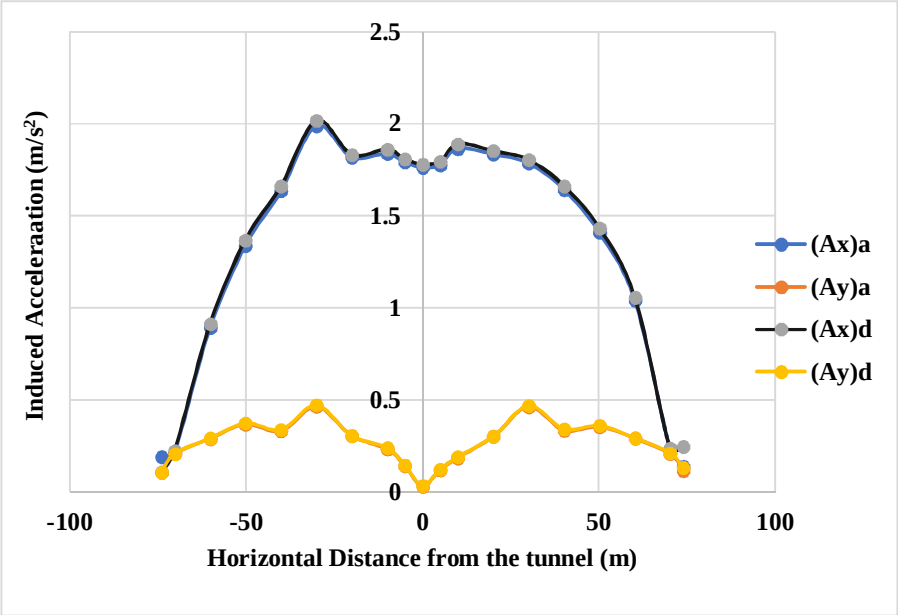

Figure 15. Displacement in soil medium and tunnel liner with different input time history.

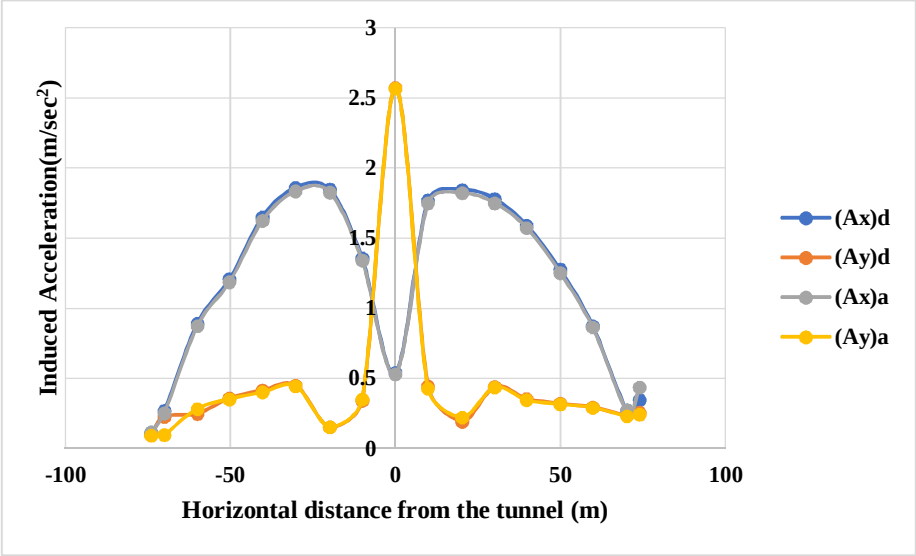

Figure 16. Displacement in soil medium and tunnel liner with different input time history.

Figures 15 and 16 show that there is no change in induced acceleration at the ground surface in the horizontal direction and same finding was found in the vertical direction in both cases. Therefore, it can be concluded that the effect of input time history on the indued acceleration at the ground surface was same for both cases.

5.4. Effect of a nearby building on induced forces in RC liner

Due to the construction of a building near the underground tunnel, the induced forces in the tunnel liner might differ from the previous case. The response of a building may also be different due to seismic loading in the presence or absence of the underground tunnel. Figure 17 shows the physical model of the site with the building.

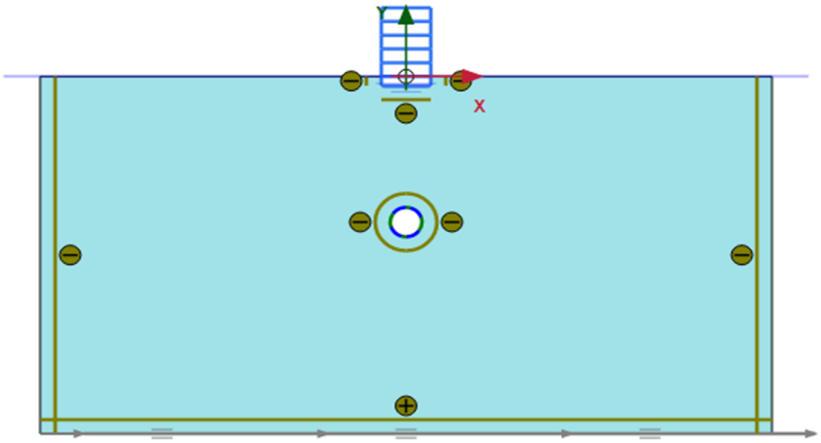

Figure 17. Physical model of the site with building.

The effect of building on the induced forces in RC liner of the tunnel, the analysis had also been done by considering building with underground tunnels. Table 9 shows all the values of induced forces in the RC liner. It can be concluded that due to the presence of a building, the value of axial force and bending moment increases significantly. Table 9 shows that in the static condition, the axial force and bending moment increased as the building was considered in the analysis. The residual forces in the RC liner of the tunnel after the shaking were also compared in Table 9. It was found that the axial force and bending moment increase when the building is present but slightly decrease in shear Force. It can be observed from Figures 18, 19, 20 that the axial force is constant along the periphery of the tunnel, and the shear stress was maximum between the spring and invert point of the liner and the bending moment was maximum at the spring point of the tunnel.

Table 9. Extreme forces develop in the RC liner of the tunnel.

Forces in RC liner	Static condition		During shaking		After shaking	
	T	T + B	T	T + B	T	T + B
Axial Force (kN/m)	2070	2268	2136	2277	2071	2268
Bending Moment (kN-m/m)	206.4	199.5	290.4	206.3	206.5	199.9
Shear Force (kN/m)	128.8	314.6	181.9	321.8	128.9	314.6

where,

T = Only tunnel considered

T + B = Tunnel and building are both considered

5.5. Tunnel's influence on building structural displacement

In this analysis, taking four working situations into consideration project status, project status one (P-1), two(P-2), three (P-3), and four (P-4), respectively, are the horizontal distance between the tunnel center and the axis of the surface building is 0, 10, 20, and 30 meters. The input seismic wave was the same (Uttarkashi earthquake,1991), inputting horizontally from the base of the FEM model.

The calculation results of each floor peak displacement of the building under five project statuses as shown in Figure 21. Figures 22 (a-d) shows the deformed mesh of the FEM model at each position.

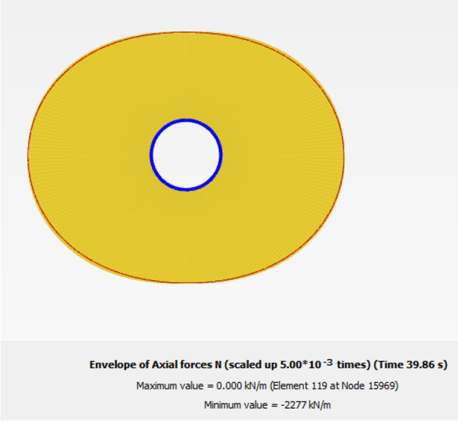

Figure 18. Maximum axial Force during shaking (T+B)

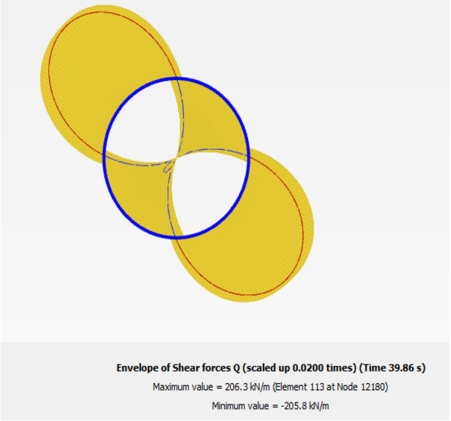

Figure 19. Maximum shear force during shaking (T+B)

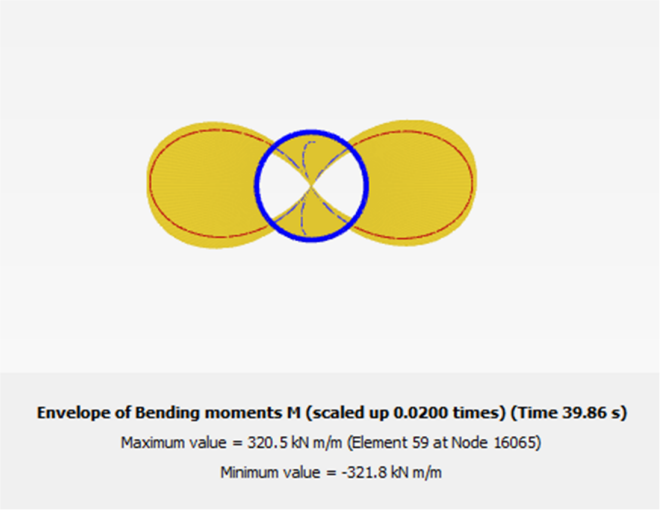

Figure 20. Maximum bending moment during shaking (T+B).

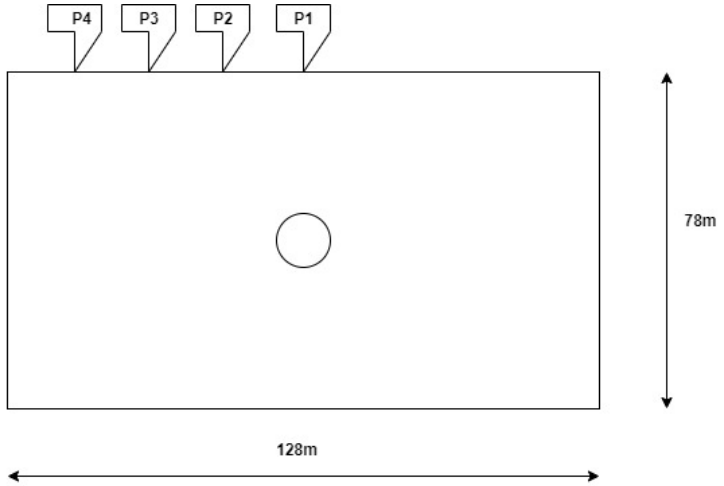

Figure 21. Diagram indicates the different positions of the building from the tunnel.

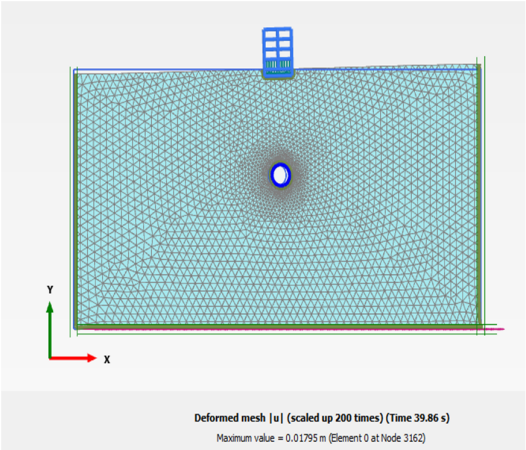

a). Deformed mesh when the building at position P-1

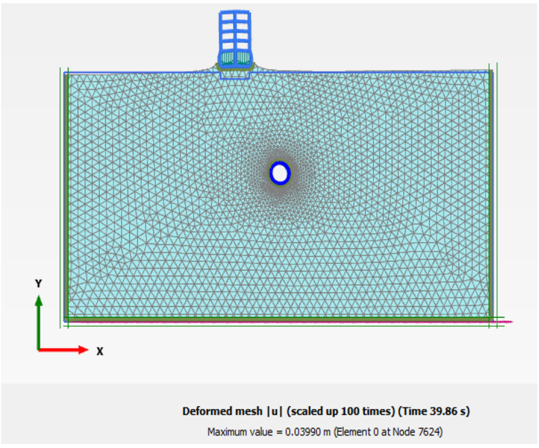

b). Deformed mesh when the building at position P-2

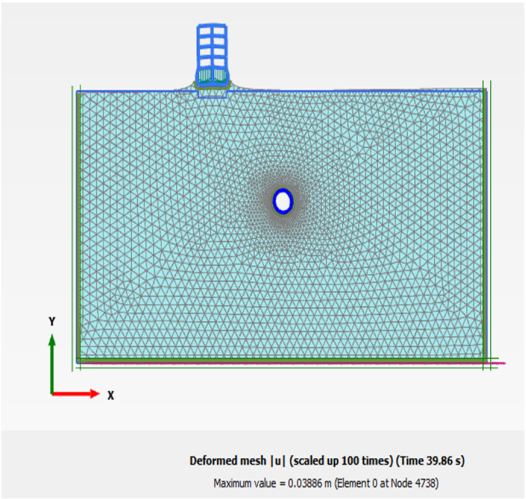

c). Deformed mesh when the building at position P-3

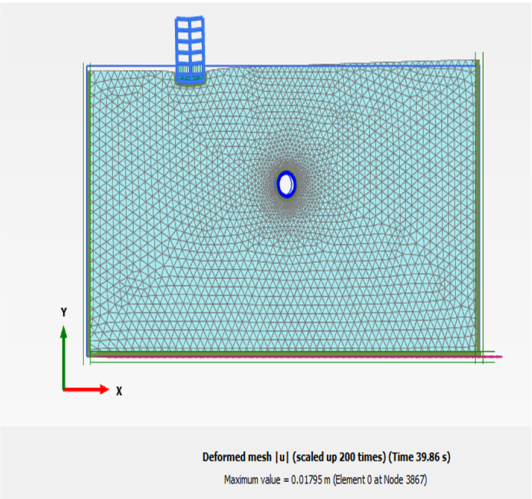

d). Deformed mesh when the building at position P-4

Figure 22. Deformed mesh at the building

Table 10. Extreme displacement in the horizontal and vertical direction in soil.

Building's position	P-1		P-2		P-3		P-4	
Story	U_x(m)	U_y(m)	U_x(m)	U_y(m)	U_x(m)	U_y(m)	U_x(m)	U_y(m)
0	0.00959	0.781	0.00529	0.744	0.00948	0.638	0.00640	0.585
1	0.00783	0.782	0.00522	0.744	0.00649	0.639	0.00594	0.586
2	0.00539	0.783	0.00377	0.745	0.00456	0.639	0.00354	0.586
3	0.00559	0.783	0.00318	0.746	0.00450	0.640	0.00267	0.586
4	0.00622	0.784	0.00280	0.746	0.00257	0.640	0.00280	0.587
5	0.006104	0.784	0.005036	0.746	0.007137	0.640	0.00567	0.587

In Table 10, the displacement of the individual storey of the building is tabulated at each position of the building concerning with tunnel's surface by applying the horizontal component of the Uttarkashi earthquake, 1991. It can be observed from the table that the displacement was maximum (in the x-direction) on the ground floor, and it decreased on the upper floors, but on the last floor, it increased.

Table 11 shows the value of the RC liner's forces when the position of the building concerns the tunnel's periphery. Table 11 shows that as the building is included, the value of axial force and bending moment increase, while the value of shear

force decreases. It can also be concluded that when the position of the building was away from the tunnel, the value of all three RC liners' forces have decreased significantly.

Table 11. Extreme forces develop in the RC Liner of the tunnel due to different positions of the building.

Building's position Forces	P-0 (no building)	P-1	P-2	P-3	P-4
Axial force (kN/m)	2136	2269	2258	2169	2138
Shear force (kN/m)	290.4	203.2	192.5	156.8	140.7
Bending moment (kN-m/m)	181.9	317.5	303.0	253.3	228.5

6. Conclusions

From this study, the following outcomes were obtained:

1. Forces in RC liners obtained in the present study are well-matched to those obtained by Penzien and Wu (1998) and Penzien (2000). Stress concentration in the case of elastic and elastoplastic analyses was also matched with the solution given by Terzaghi and Richart, and Bray (1967), respectively.
2. The vertical stress concentration and volume loss depend upon the soil medium's constitutive behavior. The applied value of volume contraction will be more significant in the case of elastoplastic behavior of the soil in comparison to elastic behavior.
3. The axial force, shear force, and bending moment increase in case of no absorbent boundary condition in the numerical model because the seismic waves return after to coincide with the non-absorbent boundary, so the domain of the numerical model should be large so that no wave can hit the tunnel lining again. If the soil medium is dampened enough, tunnel-induced forces will remain within limits, and the domain of the FEM model can be minimized.
4. The section under consideration was safe against the 1991 Uttarkashi earthquake. However, this statement was only valid for the Uttarkashi earthquake, and soil behaviour was also considered elastic.
5. It can be observed that, due to the presence of the building, the axial force and bending moment increased in tunnel's liner, and the value of all three forces reduced as the position of the building was away from the tunnel.
6. Shear force and bending moment were maximum for full slip condition between soil and tunnel lining however the effect of the interface condition on the displacement was negligible after a certain value of the interface condition.

References

[1]. Hashash, Y.M., Hook, J.J., Schmidt, B., John, I., and Yao, C. (2001). Seismic design and analysis of underground structures. Tunnelling and underground space technology, 16(4): 247-293.

[2]. Zhang, X., Jiang, Y., and Maegawa, K. (2020). Mountain tunnel under earthquake force: A review of possible causes of damages and restoration methods. Journal of Rock Mechanics and Geotechnical Engineering, 12(2): 414-426.

[3]. Owen, G.N. and Scholl, R.E., 1981. Earthquake engineering of large underground structures. Report no. FHWARD-80195. Federal Highway Administration and National Science Foundation

[4]. Gil, L.M., Hernandez, E., and De la Fuente, P. (2001). Simplified transverse seismic analysis of buried structures. Soil Dynamics and Earthquake Engineering, 21(8): 735-740.

[5]. Penzien, J. (2000). Seismically induced racking of tunnel linings. Earthquake Engineering & Structural Dynamics, 29(5): 683-691.

[6]. St John, C.M. and Zahrah, T.F. (1987). Aseismic design of underground structures. Tunnelling and underground space technology, 2(2): 165-197.

[7]. Stamos, A.A. and Beskos, D. E. (1996). 3-D seismic response analysis of long lined tunnels in half-space. Soil Dynamics and Earthquake Engineering, 15(2): 111-118.

[8]. Wang, J.N. (1993). Seismic design of tunnels: a state-of-the-art approach, monograph, monograph 7. Parsons, Brinckerhoff, Quade and Douglas Inc, New York.

[9]. Cilingir, U. and Madabhushi, S.G. (2011). A model study on the effects of input motion on the seismic behavior of tunnels. Soil Dynamics and Earthquake Engineering, 31(3): 452-462.

[10]. Lanzano, G., Bilotta, E., Russo, G., Silvestri, F., and Madabhushi, S. G. (2012). Centrifuge modeling of seismic loading on tunnels in sand. Geotechnical Testing Journal, 35(6): 854-869.

[11]. Tsinidis, G., Pitilakis, K., and Trikalioti, A.D. (2014). Numerical simulation of round robin numerical test on tunnels using a simplified kinematic hardening model. Acta Geotechnica, 9(4): 641-659.

[12]. Xu, H., Li, T., Xia, L., Zhao, J.X., Wang, D. (2016). Shaking table tests on seismic measures of a

model mountain tunnel. Tunn. Undergr. Sp. Tech. 60, 197–209.

[13]. Luzhen, J., Jun, C., and Jie, L. (2010). Seismic response of underground utility tunnels: shaking table testing and FEM analysis. Earthquake Eng. Eng. Vib. 9, 555–567.

[14]. Chen, Z., Liang, S., Shen, H., and He, C. (2018). Dynamic centrifuge tests on effects of isolation layer and cross-section dimensions on shield tunnels. Soil Dyn. Earthquake Eng. 109,173–187.

[15]. Xin, C.L., Wang, Z.Z., Zhou, J.M., and Gao, B. (2019). Shaking table tests on seismic behavior of polypropylene fiber reinforced concrete tunnel lining. Tunn. Undergr. Space Technol. 88, 1–15.

[16]. Guobo, W., Mingzhi, Y., Yu, M., Jun, W., and Wang, Y. (2018). Experimental study on seismic response of underground tunnel-soil-surface structure interaction system. Tunn. Undergr. Space Technol. 76, 145–159.

[17]. Chen, X., Shen, J., Bao, X., Wu, X., Tang, W., and Cui, H. (2023). A review of seismic resilience of shield tunnels. Tunnelling and Underground Space Technology, 136, 105075.

[18]. Tsinidis, G., Pitilakis, K., and Anagnostopoulos, C. (2016). Circular tunnels in sand: dynamic response and efficiency of seismic analysis methods at extreme lining flexibilities. Bulletin of earthquake engineering, 14, 2903-2929.

[19]. Sharma, S. and Judd, W.R. (1991). Underground opening damage from earthquakes. Engng Geol. 30, No. 3–4, 263–276.

[20]. Huang, Z.K., Pitilakis, K., Tsinidis, G., Argyroudis, S., and Zhang, D.M. (2020). Seismic vulnerability of circular tunnels in soft soil deposits: The case of Shanghai metropolitan system. Tunnelling and Underground Space Technology, 98, 103341.

[21]. Huang, J., Zhao, X., Zhao, M., Du, X., Wang, Y., Zhang, C., and Zhang, C. (2020). Effect of peak ground parameters on the nonlinear seismic response of long lined tunnels. Tunnelling and Underground Space Technology, 95, 103175.

[22]. Jiang, J., El Nggar, H. M., Xu, C., Zhong, Z., and Du, X. (2021). Effect of ground motion characteristics on seismic fragility of subway station. Soil Dynamics and Earthquake Engineering, 143, 106618.

[23]. Singh, M., Samadhiya, N.K., and Yadav, J.S. (2021). Effect of Earthquake on Underground Metro Tunnels—A Parametric Study. In Proceedings of the 1st Indo-China Research Series in Geotechnical and Geoenvironmental Engineering (pp. 1-19). Springer Singapore.

[24]. Liu, S., Yao, L., Feng, X., and Wang, P. (2022). Response Analysis of Curved Tunnel under Near-Field Long-Period Ground Motion Considering Seismic Wave Propagation Effect. Sustainability, 15(1): 60.

[25]. Rowe R (1992). Tunnel engineering in earthquake area. J Tunn Tunn 12:41–44

[26]. Lanzano, G., Bilotta, E., Russo, G., and Silvestri, F. (2015). Experimental and numerical study on circular tunnels under seismic loading. European Journal of Environmental and Civil Engineering, 19(5): 539-563

[27]. Pakbaz, M.C. and Yareevand, A. (2005). 2-D analysis of circular tunnel against earthquake loading. Tunnelling and Underground Space Technology, 20(5): 411-417.

[28]. Lotfi, M.M., Vafaeian, M., (2006). Analyzing the seismic effect on the metro tunnels in response to some known earthquakes. Tunn. Undergr. Space Technol. 21(3–4).

[29]. Kampas, G., Knappett, J.A., Brown, M.J., Anastasopoulos, I., Nikitas, N., and Fuentes, R., 2020. Implications of volume loss on the seismic response of tunnels in coarsegrained soils. Tunn. Undergr. Space Technol.

[30]. Jagdish, P.S. and Jyant, K. (2014). Stability of a circular tunnel in presence of pseudostatic seismic body forces. Tunn. Undergr. Space Technol. 42, 264–276.

[31]. Miao, Y., Yao, E., Ruan, B., and Zhuang, H., (2018). Seismic response of shield tunnel subjected. to spatially varying earthquake ground motions. Tunn. Undergr. Space Technol. 77, 216–226. https://doi.org/10.1016/j.tust.2018.04.006.

[32]. de Silva, F., Fabozzi, S., Nikitas, N., Bilotta, E., and Fuentes, R., (2021). Seismic vulnerability of circular tunnels in sand. Geotechnique. 71(11): 1056-1070.

[33]. de Silva, F., Fabozzi, S., Nikitas, N., Bilotta, E., and Fuentes, R. (2019). Site Specific Seismic Performance of Circular Tunnels in Dry Sand. In: Proceedings of VII Convegno Nazionale dei Ricercatori di Inge.

[34]. Penzien, J. and Wu, C.L. (1998). Stresses in linings of bored tunnels. Earthquake engineering & structural dynamics, 27(3): 283-300.

[35]. Hashash, Y.M., Park, D., John, I., and Yao, C. (2005). Ovaling deformations of circular tunnels under seismic loading, an update on seismic design and analysis of underground structures. Tunnelling and Underground Space Technology, 20(5): 435-441.

[36]. Ashish Chandrorkar (2021). A comprehensive report on Metro rail systems in India.

[37]. Siemiatycki, Matti (2006). Message in a Metro: Building Urban Rail Infrastructure and Image in Delhi, India". International Journal of Urban and Regional Research. **30** (2): 277–292.

[38]. Yadav, H.R. (2005). Geotechnical evaluation and analysis of Delhi metro tunnels (Doctoral dissertation).

[39]. Soni, S. (2015). Static and dynamic response of Delhi metro tunnels (Doctoral dissertation, IIT Delhi).

[40]. Iyengar, R.N. (2000). Seismic status of Delhi megacity. Current Science, 78(5): 568-574.

[41]. Draft- Hazard and Risk Assessment, http://web.delhi.gov.in/DoIT/DOIT_DM/risks%20and%20 vulnerability-1.pdf

[42]. Lysmer, J. and Kuhlemeyer, R.L. (1969). Finite dynamic model for infinite media. Journal of the engineering mechanics division, 95(4): 859-877.

[43]. BIS, I. (2000). 456 (2000) Plain and reinforced concrete-Code of Practice. Bureau of Indian Standards, New Delhi, India.

[44]. Terzaghi K, Richart FE. Stress in rock about cavities. Geotechnique 1952; 3(2):57– 90

[45]. Bray, J. (1987). Analytical and computational methods in engineering rock mechanics. Taylor & Francis.

[46]. Dhadse, G.D., Ramtekkar, G.D., and Bhatt, G. (2021). Finite element modeling of soil structure interaction system with interface: a review. Archives of Computational Methods in Engineering, 28, 3415-3432.

[47]. J.P. Carter, C.S. Desai, D.M. Potts, H.F. Schweiger, and S.W. Sloan, Computing and computer modelling in geotechnical engineering. Proc. of the Int. Conf. on Geotechnical and Geological Engineering (GeoEng2000): Melbourne, vol. I (2000): 1157-1252.

[48]. P.C.F. Ng, I.C. Pyrah, and W.F. Anderson, Assessment of three interface elements and modification of the interface element in CRISP90. Computers and Geotechnics 21 (1997): 315-339.

[49]. R. Goodman, R. Taylor, and T. Brekke, A model for the mechanics of jointed rock. Journal of Soil Mechanics and Foundations Division 99 (1968): 637-659.

[50]. R.A. Day and D.M. Potts, Zero thickness interface elements' numerical stability and application. International Journal for Numerical and Analytical Methods in Geomechanics 18 (1994): 689˚708.

[51]. Hashash YMA, Hook JJ, Schmidt B, and Yao JI-C. Seismic design, and analysis of underground structures. Tunnelling and Underground Space Technology 2001; 16:247–93

[52]. Merritt, J.L., Monsees, J.E., and Hendron, A.J., (1985). Seismic design of underground structures: Proc of the 1985 Rapid Excavation and Tunneling Conference, New York. International Journal of Rock Mechanics and Mining Science & Geomechanics Abstracts, Volume 23, Issue 6, 255-282.

Appendix A: Volume contraction/volume loss (V_L)

Numerous solutions for the distribution of stresses in elastic media have been reported. Still, the solutions mentioned below include only those important and relevant to evaluating stresses and displacements around underground openings.

For the applied stresses (as in situ) far away from the origin in the x and z direction, σ_x and σ_z Respectively, the expressions for radial, tangential, and shear at the element "A" are expressed as:

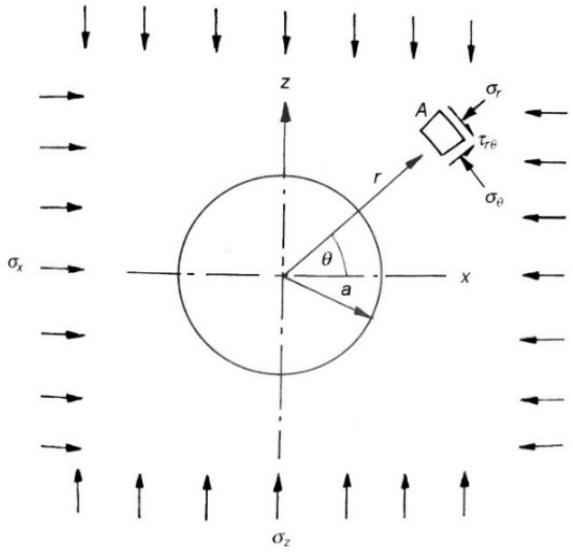

Figure 19. A circular hole in an infinite plate.

$$\sigma_r = \frac{1}{2}(\sigma_x + \sigma_z)\left(1 - \frac{a^2}{r^2}\right) + \frac{1}{2}(\sigma_x - \sigma_z)\left(1 + \frac{3a^4}{r^4} - \frac{4a^2}{r^2}\right)cos2\theta \quad (10)$$

$$\sigma_\theta = \frac{1}{2}(\sigma_x + \sigma_z)\left(1 + \frac{a^2}{r^2}\right) - \frac{1}{2}(\sigma_x - \sigma_z)\left(1 + \frac{3a^4}{r^4}\right)cos2\theta \quad (11)$$

$$\tau_{r\theta} = -\frac{1}{2}(\sigma_x - \sigma_z)\left(1 - \frac{3a^4}{r^4} + \frac{2a^2}{r^2}\right)sin2\theta \quad (12)$$

Where

σ_r = radial stress
σ_θ = tangential stress
$\tau_{r\theta}$ = shear stress
σ_x = horizontal pressure
σ_z = geostatistical overburden pressure
a = radius of the circular opening
r = radial distance from the center of the opening
θ = central angle with the x-axis

Terzaghi and Richart [26] used Krish's solutions (Equations (10) to (12)) to study the stress distribution around circular openings. The horizontal and vertical stresses are transformed from radial and tangential stresses at the crown and the springing levels with the help of the following equations:

$$\sigma_h = \frac{\sigma_\theta + \sigma_r}{2} + \frac{\sigma_\theta - \sigma_r}{2}cos2\theta + \tau_{r\theta}sin2\theta \quad (13)$$

$$\sigma_v = \frac{\sigma_\theta + \sigma_r}{2} - \frac{\sigma_\theta - \sigma_r}{2}cos2\theta - \tau_{r\theta}sin2\theta \quad (14)$$

$$\tau_{vh} = -\frac{\sigma_\theta - \sigma_r}{2}sin2\theta + \tau_{r\theta}cos2\theta \quad (15)$$

Vertical stress concentration at a particular point was calculated by using Equation No. 14 in this study.

Appendix B: Ovaling deformation of circular tunnels

The response of a tunnel lining is a function of the compressibility and flexibility ratios of the structure and the in-situ overburden pressure and at-rest coefficient of earth pressure of the soil. The stiffness of a tunnel relative to the surrounding ground is quantified by the compressibility and flexibility ratios (C and F), which are measures of the extensional stiffness and the flexural stiffness (resistance to Ovaling), respectively, of the medium relative to the lining [52]:

$$C = \frac{E_m(1-\upsilon_l^2)r}{E_l t(1+\upsilon_m)(1-2\upsilon_m)} \quad (16)$$

$$F = \frac{E_m(1-\upsilon_l^2)r^3}{6E_l I(1+\upsilon_m)} \quad (17)$$

where E_m is the modulus of elasticity of the medium, I is the moment of inertia of tunnel lining (per unit width), r is the radius of the circular tunnel, and t is the thickness of the tunnel lining.

Assuming full-slip condition, the maximum axial force and bending moment can be expressed as (Wang, 1993):

$$\frac{\Delta d}{d} = \pm\frac{1}{3}K_1 F\gamma_{max} \quad (18)$$

$$T_{max} = \pm\frac{1}{6}K_1\frac{E_m}{(1+\nu_m)}r\gamma_{max} \quad (19)$$

Where

$$K_1 = \frac{12(1-\nu_m)}{2F+5-6\nu_m} \quad (21)$$

Penzien and Wu [16] developed similar analytical solutions for axial force, shear force, and bending moment in the tunnel lining due to racking deformations. Assuming full slip condition, solutions for axial force, moment, and shear force in circular tunnel linings caused by soil-structure interaction during a seismic event are expressed as:

$$\pm\Delta d_{lining}^n = \pm R^n \Delta d_{free-field} \quad (22)$$

$$T_{max} = -\frac{12E_l\Delta d_{lining}^n}{d^3(1-\nu_l^2)} \quad (23)$$

$$M_{max} = -\frac{6E_l I\Delta d_{lining}^n}{d^2(1-\nu_l^2)} = \frac{d}{2} * T_{max} \quad (24)$$

$$V_{max} = -\frac{24E_l I\Delta d_{lining}^n}{d^3(1-\nu_l^2)} = 2 * T_{max} \quad (25)$$

The lining-soi; racking ratio under normal loading only is defined as:

$$R^n = \pm\frac{4(1-\nu_m)}{(\alpha^n+1)} \quad (26)$$

$$\alpha^n = \frac{12E_l I(5-6\nu_m)}{d^3 G_m(1-\nu_l^2)} \quad (27)$$

In the case of the no-slip condition, the formulation is presented as follows:

$$\pm\Delta d_{lining} = \pm R\Delta d_{free-field} \quad (28)$$

$$T_{max} = -\frac{24E_l\Delta d_{lining}^n}{d^3(1-\nu_l^2)} \quad (29)$$

$$M_{max} = -\frac{6E_l I\Delta d_{lining}^n}{d^2(1-\nu_l^2)} = \frac{d}{2} * T_{max} \quad (30)$$

$$V_{max} = -\frac{24E_l I\Delta d_{lining}^n}{d^3(1-\nu_l^2)} = 2 * T_{max} \quad (31)$$

where,

$$R = \pm\frac{4(1-\nu_m)}{(\alpha+1)} \quad (32)$$

$$\alpha = \frac{24E_l I(3-4\nu_m)}{d^3 G_m(1-\nu_l^2)} \quad (33)$$

Combined stress σ from axial force and bending moment

$$\sigma = \frac{T}{A_l} + \frac{MY}{I} \quad (34)$$

مطالعه‌ای بر روی تحلیل لرزه‌ای تونل‌های زیرزمینی برای متروی دهلی

راهول شاکیا* و مانندرا سینگ

گروه مهندسی عمران، موسسه ملی فناوری هامیرپور، هیماچال پرادش، هند

ارسال 2023/01/11، پذیرش 2023/06/04

* نویسنده مسئول مکاتبات: rahulshakya4050@gmail.com

چکیده:

به دلیل شهرنشینی سریع، کمبود سطوح بالای زمین وجود دارد. بنابراین برای کاهش این کمبود سطح زمین، تونل‌های زیرزمینی برای اهداف حمل و نقل در زیر سازه ساخته می‌شود. در نتیجه، درک چگونگی تأثیر زلزله بر تونل‌های زیرزمینی بسیار مهم است تا بتوان جان مردم را نجات داد و سطح خدمات را حفظ کرد. سازه‌های زیرزمینی را نمی‌توان کاملاً از اثرات لرزش زمین مصون دانست، همانطور که زلزله کوبه (1995)، زمین‌لرزه چی-چی (1999)، و زلزله نیگاتا (2004)، که برخی از سازه‌های زیرزمینی به شدت آسیب دیدند، نشان می‌دهد. یک بخش معمولی در Chandani Chowk از تونل‌های DMRC (شرکت راه‌آهن مترو دهلی)، دهلی نو، هند، با استفاده از روش اجزای محدود تحلیل شده است. پاسخ سیستم تونل خاک برای زلزله اوتارکاشی (1991) به صورت حداکثر نیروهای القا شده در لاینر RC تونل، جابجایی، شتاب القایی و تنش‌ها مشخص شده است. نتایج با راه حل‌های بسته موجود مقایسه شده است. مطالعات پارامتری با در نظر گرفتن پارامترهای مختلف از جمله اثر انقباض (افت حجم)، تأثیر شرایط مرزی و میرایی، تأثیر وضعیت فصل مشترک بین خاک و تونل، تأثیر تاریخچه زمانی جابجایی و تأثیر ساختمان مجاور نیز انجام شده است. نیروهای موجود در لاینرهای RC و تمرکز تنش به‌دست‌آمده در مطالعه حاضر، به خوبی با نیروهای به‌دست‌آمده توسط محلول‌های بسته موجود مطابقت دارند. تمرکز تنش عمودی و کاهش حجم به رفتار سازنده محیط خاک بستگی دارد. بخش مورد بررسی در برابر زلزله سال 1991 اوتارکاشی ایمن بود. همچنین مشاهده می‌شود که به دلیل وجود ساختمان، نیروی محوری و لنگر خمشی در لاینر تونل افزایش یافته و با دور شدن موقعیت ساختمان از تونل، مقدار هر سه نیرو کاهش یافته است. نیروی برشی و لنگر خمشی برای شرایط لغزش کامل بین پوشش خاک و تونل حداکثر بود، اما تأثیر شرایط فصل مشترک بر جابجایی پس از مقدار معینی از شرایط فصل مشترک ناچیز بود.

کلمات کلیدی: تحلیل لرزه‌ای، مدل عددی، روش اجزای محدود، زلزله اوتارکاشی.